Automatic Recovery of Fixed-wing Unmanned Aerial Vehicle Using Bluetooth Angle-of-Arrival Navigation*

Martin L. Sollie[1], Kristoffer Gryte[1], Torleiv H. Bryne[1], Tor A. Johansen[1,2]

***Abstract*— We demonstrate that the Bluetooth 5.1 Angle-of-Arrival feature can be used as a navigation system for automatic recovery of a fixed-wing unmanned aerial vehicle (UAV), guiding the UAV into an arrest system such as a suspended net, independently from global navigation satellite systems (GNSS). The effect of multipath signal interference on the elevation angle estimate is handled by a constant offset calibration. In field experiments, we demonstrate approach path following using a Skywalker X8 fixed-wing UAV and a Bluetooth antenna array. For 39 approach repetitions the resulting impact positions 40m in front of the array had standard deviations of 0.41m horizontally and 0.32m vertically according to precise RTK GNSS positioning used for comparison.**

I. Introduction

A key to enabling fully automated fixed-wing UAV flights is the automatic recovery at the end of the mission, where a skilled pilot is typically used today. An arresting system such as a suspended net [1], [2], [3] or wire [4], [5] can be used for this purpose, requiring only a small ground area. To perform the recovery, a system for navigation relative to the arrest system is required.

Automatic recovery of fixed-wing unmanned aerial vehicles in a moving net, using moving-base Real-Time-Kinematic (RTK) Global Navigation Satellite System (GNSS) receivers for navigation relative to the arrest system, was demonstrated in [3], [6]. RTK GNSS was used to find both the orientation of the recovery net and the very accurate and precise position of the UAV relative to the net. RTK processing requires good quality GNSS signal reception, and due to the low power of GNSS signals, unintentional or intentional signal interference can occur. It is therefore desirable to have alternatives for local navigation in addition to GNSS for increased robustness, especially in the final phase of recovery where high precision is important.

Camera-based relative navigation [7], [8] can also be used for arrest system recovery [2], [9], [10], measuring the directions and range from a visual sensor mounted on the UAV to known visible features on or close to the arrest system, or from one or more sensors on the arrest system to the UAV. The downside of visual navigation is the requirement for visibility, with limited usefulness in conditions such as darkness, fog, snow, dust, or rain.

*The research is sponsored by the Research Council of Norway through the Centre of Excellence funding scheme (NTNU-AMOS), grant 223254, and the PARNAV project, grant 338789.

[1]Department of Engineering Cybernetics, Norwegian University of Science and Technology, Trondheim, Norway.

[2] Corresponding author: Tor.Arne.Johansen@ntnu.no

Ultra-wideband (UWB) radio can be used for UAV positioning, using trilateration with range measurements to fixed independent anchors [11], [12]. To estimate position from these range measurements, the anchors should be positioned to create a sufficiently good measurement geometry, with a low dilution of precision (DOP), the same as is the case for GNSS pseudorange measurements. Such anchor positioning results in a larger infrastructure footprint than for antenna arrays, although it is also possible to use UWB for direction finding using arrays [13], [14].

UAV flight using phased array radio for navigation, instead of GNSS, was demonstrated in [15], using a powerful long-range system operating on a licensed frequency band. The array was used to determine the azimuth angle from a known location to the UAV. To estimate the position, range measurements from the same system were utilized in combination with the azimuth angle and barometric height, making beyond-line-of-sight flight possible.

Bluetooth direction finding using antenna arrays is another alternative for radio navigation, operating in the unlicensed 2.4 GHz industrial, scientific and medical (ISM) band. Bluetooth uses a single receiver and signal switches to sequentially connect the receiver to each element, while UWB arrays use separate receiver channels for every element. The cost for a UWB array with many elements will therefore likely be higher than for Bluetooth, although the high sampling rate of UWB can result in improved performance for multipath propagation conditions. A benefit of using Bluetooth is that the low cost of the equipment enables widespread use, [16], [17]. In [18] we demonstrated navigation using Bluetooth Angle-of-Arrival (AoA) direction finding at up to 700 m distance. The angular direction estimate did not degrade significantly with range, even with received signal strength just over the receiver sensitivity threshold of -93 dBm, although packet loss did increase at longer ranges, especially beyond 500 m. Reflections from the ground interfering with the directly propagating signal, resulting in elevation angle estimate errors, were found to be the main error source, which was demonstrated using simulations and field experiments.

Bluetooth direction finding can be used as an addition to GNSS for navigation relative to the arrest system, providing information of the offset from the desired path. The recovery concept using Bluetooth involves placing an antenna array behind a recovery net, as illustrated in Fig. 1. Since the Bluetooth specification does not at present provide accurate range measurements, the

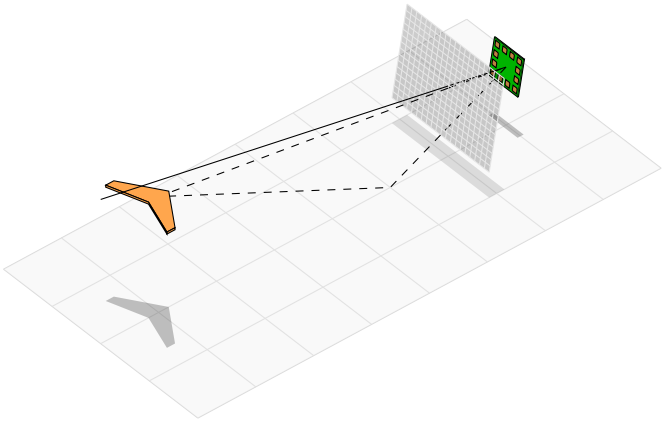

Fig. 1 Illustration of the recovery concept: a net is placed in front of the array, and a desired path/glideslope (solid line) guides the UAV directly towards the array, through the net. The UAV, which is illustrated as flying slightly below the glideslope, transmits a signal to the array. The array measurements are used to estimate the direction from the array to the UAV, which is used by the UAV controllers to steer onto the desired path. The signal can propagate both directly to the array and as a reflection off the ground surface (dashed lines), which can affect the direction estimate.

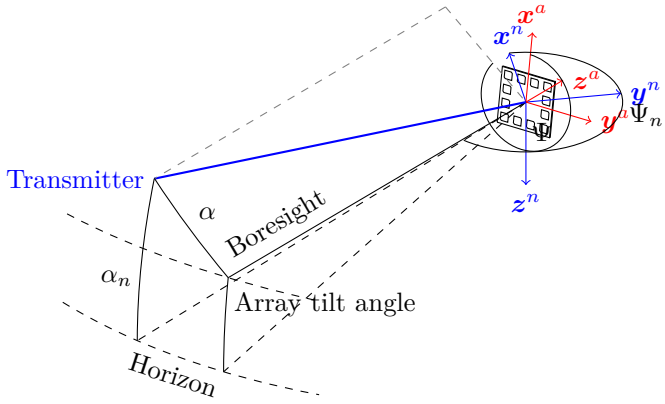

Fig. 2 Illustration of array setup with coordinate frames $\{a\}$ and $\{n\}$, and the angle notation used for directions from the array. $-\boldsymbol{z}^a$ is the boresight direction, where the antenna elements have the maximum gain.

position cannot be estimated without aiding from other sensors. The UAV, therefore, follows a path directly towards the array, enabling control based on direction, without the need for a distance estimate.

The main contribution of this paper is demonstrating the practical use of Bluetooth AoA navigation for control of a fixed-wing UAV, performing a maneuver that enables automatic recovery in a stationary arrest system. This is intended as a proof of concept and includes field experiments where AoA measurements are used in the control loop instead of GNSS in a standard Cube Black autopilot for a Skywalker X8 UAV at a range of up to 480m. Methods to handle ground reflection multipath are considered. This paper is based on [19], where further information is given.

II. Preliminaries

The antenna array coordinate frame $\{a\}$ and the navigation coordinate frame $\{n\}$ are illustrated in Fig. 2. Frame $\{n\}$ has its origin coincident with $\{a\}$, but with axes pointing towards North-East-Down (NED). Directions in the antenna frame are parameterized using the polar angle α and the azimuthal angle Ψ. α is the angle of incidence with the array plane, which is 0 in the boresight direction and $\frac{\pi}{2}$ for a direction in the array xy-plane. Ψ is measured in the antenna xy-plane about $\boldsymbol{z}^a$ using the right-hand rule, with $\Psi = 0$ for the direction $\boldsymbol{x}^a$. In $\{n\}$ we have the azimuth angle Ψ_n measured relative to North and elevation angle α_n measured from the horizontal tangent plane. Estimated values are denoted $\hat{\Psi}_n$ and $\hat{\alpha}_n$. The rotation matrix from the UAV's body-fixed frame $\{b\}$ to $\{n\}$, $\boldsymbol{R}_b^n \in SO(3)$, is parameterized by the ZYX Tait-Bryan Euler angles $\Theta = \begin{bmatrix}\phi & \theta & \psi\end{bmatrix}^\top$, where ϕ is the roll or bank angle, θ the pitch angle, and ψ is the heading or yaw angle. The direction of the UAV velocity vector in the horizontal plane is the course angle χ. The direction of a flight path in the horizontal plane is denoted χ_p. Subscript d, e.g. ϕ_d, denotes desired values for control.

III. Navigation using Bluetooth Angle-of-Arrival estimation

Direction finding using AoA estimation involves an antenna transmitting a signal, and an array of receiver antennas all receiving the same signal. For Bluetooth direction finding the signal transmitted is a pure sinusoidal carrier, the Constant Tone Extension (CTE) at the end of a Bluetooth packet. The phase difference between the received signal and an internal reference oscillator is found for all receiver antennas. Relative differences in the phase angles indicate differences in distance between the transmitter and each element. The signal radiates spherically from the transmitter, but if the distance between array and transmitter is very large relative to the size of the array, the wavefront appears nearly planar when received, which simplifies processing by making it range-independent. Based on the measured distance differences for the antennas, the direction from which the signal arrives can be found. The measurement processing for Bluetooth AoA estimation uses the conventional Bartlett beamformer, see [18]. The output of the complete estimation method is an antenna-frame direction α, Ψ. Using the known orientation of the array, this is transformed to navigation-frame direction parameters α_n, Ψ_n, which are used for the UAV control.

It was shown in [18] that a source of error in the elevation angle estimate α_n was the signal reflected from the ground surface and received by the array antennas as an addition to the direct signal. The reflected signal causes interference, which results in an elevation-angle-dependent error in the elevation angle estimate. This

error depends on several factors including the array size, its height over the ground, and the reflectivity of the ground surface. For uneven ground surfaces, different azimuth angles can also result in different elevation errors. Removing the elevation error by calibration is not always possible, as the same measurement can in some cases be the result of more than one elevation angle. This phenomenon can be seen by plotting the elevation angle estimate as a function of the measured elevation from another system such as RTK GNSS, which provides relative positioning with errors on the centimeter level. Fig. 3a shows an example plot from a field experiment, where the relationship between RTK elevation and Bluetooth elevation, for each of the three Bluetooth channels used, appears to have a one-to-one relation. A calibration correcting most of the systematic errors should then be possible.

Fig. 3b on the other hand shows the plot from a different field experiment where the array was placed further from the ground. For RTK-indicated elevation angles below 20°, a Bluetooth measurement cannot unambiguously be corrected to the true elevation angle in this case, at least when considering only a single measurement at a single frequency. This makes it challenging to use this setup for standalone navigation at low elevation angles. Even for equipment setups where calibration is possible, the calibration transform will be a function of ground reflectivity, meaning that surface material, such as grass, gravel, soil, snow, or water, and its moisture content, can make it necessary to calibrate for different conditions.

The glideslope angle for the descent of a fixed-wing aircraft is typically low to avoid excessive airspeed. From field experiments, it appears that the elevation error due to multipath is greatest at low elevation angles, without significant systematic error above approximately 20° to (numerical range) 25° for the array used. To impact the recovery arrest system, in this case a net suspended in front of the array, we want to fly along a straight-line path with a downward slope, using the Bluetooth direction measurements as the basis for guidance and control. The effect of multipath must be taken into account to make following the desired path with sufficient accuracy possible.

A straight-line path directly to the array will have a constant elevation angle α_n. The position of the net center, the glideslope angle, and the position of the array must be compatible, while also considering the multipath error the array position will produce. For a non-zero descent angle it is possible to combine a low array height with a reasonable net height, but the higher the desired net intersection point and lower the angle, the further behind the net the array must be placed. For example, a 4° net intersection slope as used for the X8 UAV in [3], with a net height of 3m and an array with its center 0.15m over the ground, requires the array to be placed approximately 41m behind the net. At this distance, the array orientation must be very accurately aligned to ensure that the glideslope intersects the desired net

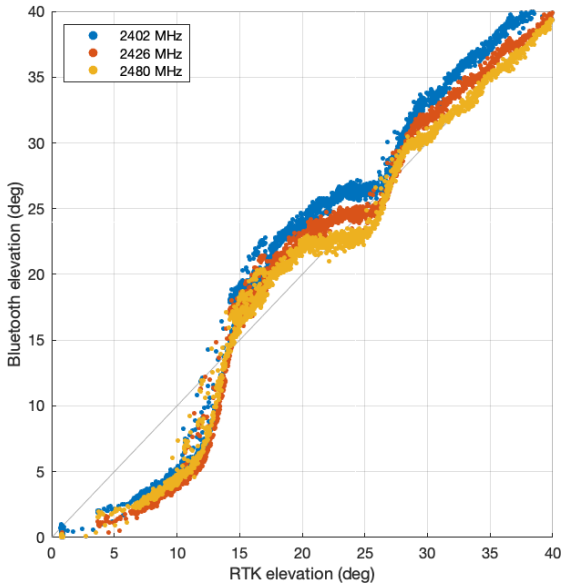

(a) Antenna array center approximately 0.15m above the ground.

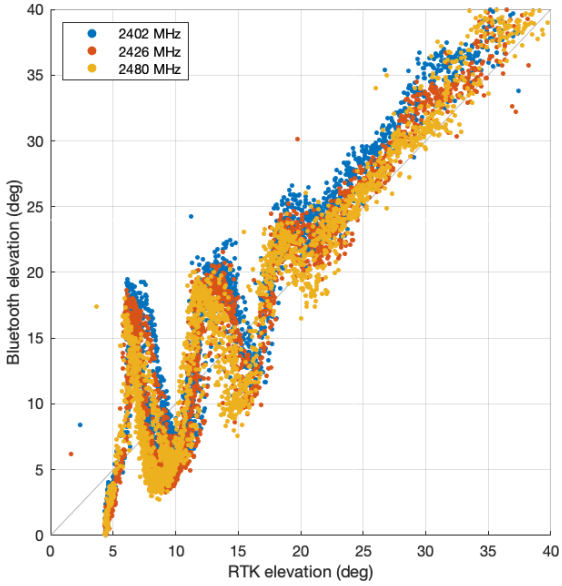

(b) Antenna array center approximately 0.5m above the ground.

Fig. 3 Effect of multipath on elevation estimate.

impact point, which is less critical with the array close to the net. Increasing the array height over ground allows the array to be placed closer to the net, but may have undesirable effects on the elevation angle multipath error [18]. Increasing the vertical size of the array can reduce this error [20].

The measurement uniqueness required for calibration limits the height the array can be placed above ground in order to make an elevation angle calibration possible. Therefore, we use an array mounted on a platform close to the ground in the experiments. To follow a glideslope with a constant elevation angle, the calibration only needs to be accurate at the angle chosen, with reasonable

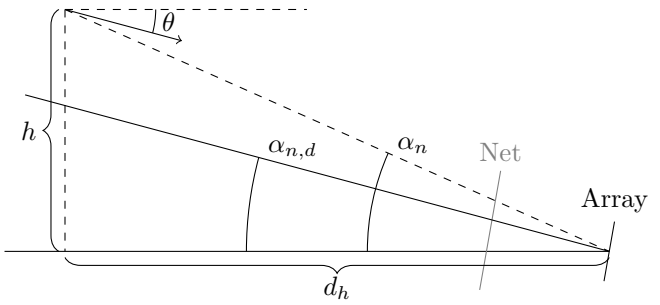

Fig. 4 Longitudinal geometry with the UAV (on the left, not shown) has altitude h and pitch angle θ, and a glideslope angle α_n with desired glideslop angle $\alpha_{n,d}$ towards the net and antenna that are shown on the right side.

errors around it locally. The simplest such calibration is a constant offset for each of the frequency channels used, which is reasonable if the gradient of the measured elevation angle with respect to the true angle is close to unity.

IV. Guidance and control

We assume that the UAV flight controller estimates attitude using an IMU and a magnetometer, and uses these to handle low-level roll and pitch control, allowing us to command desired roll and pitch angles. A heading angle estimate is assumed available for the higher-level control, in addition to airspeed measurements from a pitot tube. To know the desired flight direction when exactly on the desired path, the array is mounted with a known azimuth angle and upwards pitch angle. The UAV's course angle χ is not assumed available, only the heading ψ. Wind perpendicular to the approach path causes the UAV to crab, with $\chi \neq \psi$. The crab angle of the UAV due to crosswind is compensated by using integral action in the controllers.

A. Airspeed control

To maintain airspeed, the throttle is commanded using a PI controller with the measured airspeed $\hat{V}_a$ and the desired airspeed $V_{a,d}$, with the error $\tilde{V}_a = V_{a,d} - \hat{V}_a$,

$$T = k_{(T,V,p)}\tilde{V}_a + \int k_{(T,V,i)}\tilde{V}_a dt + T_{\text{trim}}, \qquad (1)$$

where $k_{(T,V,p)}$ and $k_{(T,V,i)}$ are proportional and integral gain parameters, respectively, and T_{trim} is a throttle trim parameter.

B. Angle-based line-following

Without knowledge of the distance between the array and UAV, we can follow a path towards the array with a desired glideslope using only angle measurements.

1) Longitudinal control: The longitudinal geometry is illustrated in Fig. 4. A pitch controller capable of following a glideslope is

$$\begin{aligned}\theta_d &= -\alpha_{n,d} - k_{(\theta,\alpha,p)}(\hat{\alpha}_n - \alpha_{n,d}) \\ &\quad - \int k_{(\theta,\alpha,i)}(\hat{\alpha}_n - \alpha_{n,d})dt + k_{(\theta,q,d)}\hat{q} + \theta_{\text{trim}} \qquad (2)\end{aligned}$$

where θ_d is the pitch setpoint sent to the low-level pitch controller running on the flight controller. $\alpha_{n,d}$ is the desired elevation angle, $\hat{q}$ is the angular rate estimate in the $\boldsymbol{y}^b$ direction (essentially the pitch rate for zero roll angle), θ_{trim} is the angle-of-attack at trim flight condition, and $k_{(\theta,\alpha,p)}$, $k_{(\theta,\alpha,i)}$ and $k_{(\theta,q,d)}$ are proportional, integral and damping gain parameters.

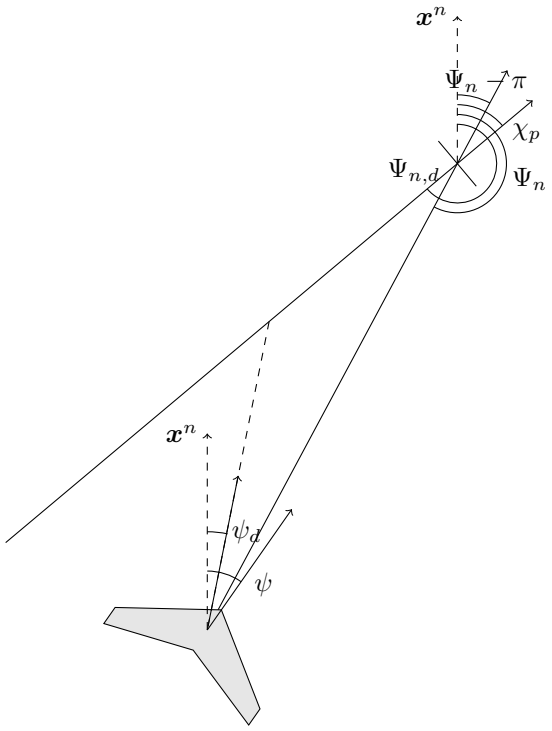

Fig. 5 Lateral geometry, where the UAV is in the lower left part and the antenna array is in the upper right part.

2) Lateral control: The lateral geometry is illustrated in Fig. 5. The lateral control consists of two steps: first, the desired flight direction is determined, and second, the desired roll angle is computed from the error between the desired and actual flight direction. The desired course angle could be computed as

$$\chi_d = (\Psi_{n,d} - \pi) + k_{(\chi,\Psi_n,p)}(\hat{\Psi}_n - \Psi_{n,d}), \qquad (3)$$

where $\Psi_{n,d}$ is the desired azimuth angle, the direction from which is assumed we want to fly towards the array. For $k_{(\chi,\Psi_n,p)} = 1$ we would aim directly towards the array without converging onto the desired path $\chi_p = \Psi_{n,d} - \pi$. Thus $k_{(\chi,\Psi_n,p)} > 1$ would be required for convergence. Ideally, the desired direction would be a course angle, but since we do not assume access to course angle estimates, the desired direction is a heading angle, where an integral is used to account for wind. The desired heading angle

can be computed as

$$\begin{aligned}\psi_d &= (\Psi_{n,d} - \pi) + k_{(\psi,\Psi_n,p)}(\hat{\Psi}_n - \Psi_{n,d}) \\ &\quad + \int k_{(\psi,\Psi_n,i)}(\hat{\Psi}_n - \Psi_{n,d})dt \end{aligned} \quad (4)$$

An issue with this very simple controller is that the proportional term $k_{(\psi,\Psi_n,p)}(\hat{\Psi}_n - \Psi_{n,d})$ can make the UAV fly away from the array for large initial azimuth errors or controller gain, $|k_{(\psi,\Psi_n,p)}(\hat{\Psi}_n - \Psi_{n,d})| > \frac{\pi}{2}$. Therefore, the controller gain would be limited by the maximum azimuth error allowed. A modification that avoids this problem is to instead use

$$\begin{aligned}\psi_d &= (\Psi_{n,d} - \pi) + \tan^{-1}(k_{(\psi,\Psi_n,p)} \tan(\hat{\Psi}_n - \Psi_{n,d})) \\ &\quad + \int k_{(\psi,\Psi_n,i)}(\hat{\Psi}_n - \Psi_{n,d})dt. \end{aligned} \quad (5)$$

In this case the parameter $k_{(\psi,\Psi_n,p)}$ becomes a inverse fractional lookahead distance. It can therefore not turn away from the array even for high gains and azimuth errors. The effect of using control based on azimuth and elevation angles is that the controller becomes more aggressive as the range decreases, when considering distance errors from the desired point on the path.

Using the desired heading angle ψ_d and the estimated heading angle ψ from the flight controller, a desired roll angle ϕ_d can be computed as $\phi_d = \text{atan}(k_{(\phi,\psi,p)}(\psi_d - \hat{\psi}))$, where $k_{(\phi,\psi,p)}$ is a tuning parameter.

V. Implementation

The electronics hardware used is the same as in [18], but will be briefly re-introduced here.

A. Ground antenna equipment

Fig. 6 show a schematic for the hardware components placed on the ground. The array is a Nordic Semiconductor experimental reference design using 12 truncated corner right-handed circular polarization (RHCP) patch antennas in a square 15x15cm pattern, with 5cm antenna spacing, controlled and sampled by an nRF52833 board. The advertising channels with frequencies 2402 MHz, 2426 MHz and 2480 MHz are used in a connectionless configuration. Bluetooth was only used for direction estimation and not as a vehicle telemetry and command link. The nRF52833 board is connected to a SentiBoard [21], which works as a USB sensor interface for the Beaglebone Black single-board computer. The data is parsed in DUNE [22], and forwarded to the payload computer on the vehicle, where the direction estimation runs.

A uBlox ZED-F9P GNSS receiver with a helix antenna is used as a Real-Time-Kinematic (RTK) base, for use in evaluation of the positioning performance of the Bluetooth system. The Beaglebone Black is connected to a Ubiquiti Rocket M5 radio using ethernet, for communication with the UAV and a ground station computer used for system monitoring.

B. UAV payload

A directional TrueRC Canada X-AIR 2.4GHz RHCP antenna is used. The antenna is specified to have a gain

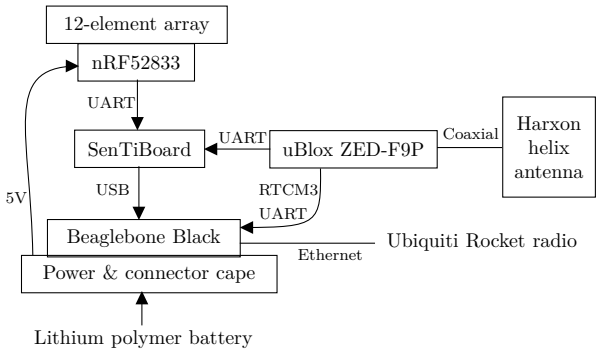

Fig. 6 Ground hardware schematic

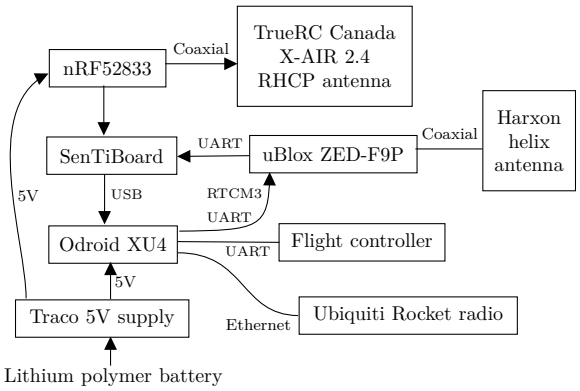

Fig. 7 UAV payload hardware schematic

of 8 dB, a −3 dB beamwidth of 75° and performance equal to an omnidirectional antenna in a 120° beam [23]. The antenna is connected to the nRF52833 transmitter board using a coaxial cable, see Figure 7. A uBlox ZED-F9P GNSS receiver with a helix antenna is used on the UAV, receiving RTCM3-format reference measurements from the base antenna mounted on the ground. This is only used for calibration of the Bluetooth system and evaluation of Bluetooth navigation performance, not for control. The RTK GNSS setup yields very accurate and precise estimates of the UAV's position relative to the GNSS antenna on the ground, with position errors on the centimeter level. The transmitter broadcasts advertising packets with a CTE at a rate of 10 Hz. The SentiBoard outputs measurements from all connected sensors to the Odroid XU4 computer where they are both logged for later analysis and parsed for real-time use.

C. Software architecture

The UAV net recovery involves software running on and communicating between several different hardware components. DUNE [22], a part of the LSTS Toolchain, is used as a robotic middleware for implementing the algorithms used in a modular fashion. Fig. 8 shows a schematic illustrating the flow of data between the components and the most important tasks running in DUNE on the UAV and ground computers.

The packets from the receiver board are parsed in DUNE on the Beaglebone Black and forwarded to

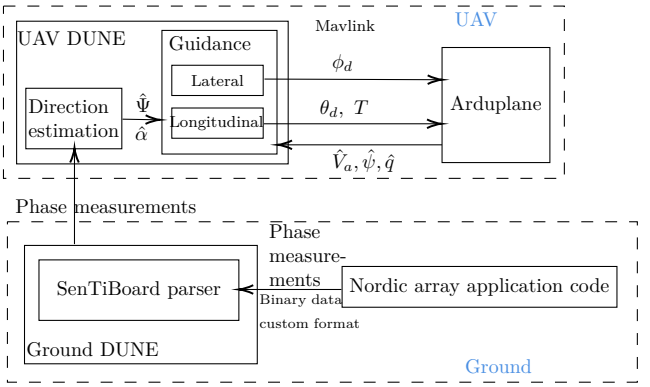

Fig. 8 Main software components for Bluetooth net recovery

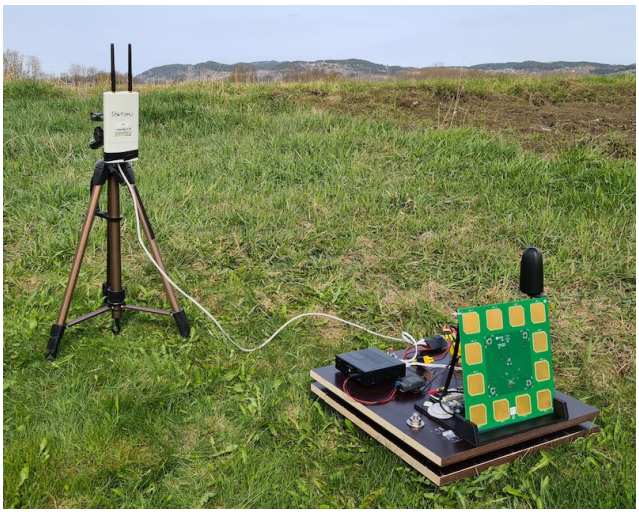

Fig. 9 Setup of antenna array for fixed-wing UAV recovery. The Bluetooth antenna array and other ground hardware used for localization is shown on the right side, and the radio communication system is on the tripod shown on the left side.

the UAV. Direction estimation using the conventional beamformer method [18] is then performed on the Odroid XU4, using a resolution of 0.1° for Ψ and 0.05° for α. The direction estimation result is sent to the guidance and control task where the lateral and longitudinal controllers run, sending desired roll and pitch angles, as well as a throttle command, using the SET_ATTITUDE_TARGET Mavlink message to the Cube Black flight controller, which handles the low-level control of the elevon control surfaces.

VI. Field experiments

In order to perform a large number of recovery maneuvers efficiently when using Bluetooth direction estimates for control, tests are performed without a physical net and with the approach aborted before reaching the array. In this way, the UAV can pass through the location where the net would be suspended without having to re-launch the UAV for every attempt.

Fig. 9 shows the ground hardware setup at the end of a grass field. The bottom part of the array platform was pushed into the soil for stability, and the top plate was leveled using the bubble level on the array holder. After this, it was assumed that the array had an upwards pitch of 10 degrees and zero roll angle.

For array azimuth angle calibration, the UAV was placed on the field on a stand keeping it raised from the ground, with the nose of the UAV, containing the transmitter antenna, pointed towards the array. The azimuth angle assumed in software was then adjusted until azimuth angles for RTK GNSS and Bluetooth measurements matched. The three Bluetooth channels showed minor azimuth angle disagreement, but this was not accounted for in the experiments.

Elevation angle offsets were identified initially on the ground by holding the UAV in front of the array at an RTK-indicated elevation angle of 9°, corresponding to the desired glideslope angle, and then reading the Bluetooth elevation estimates for each channel. The offset values were further adjusted while flying, although adjusting while performing approach maneuvers affects the actual elevation angle flown and thereby the offset required for correction, making it an iterative process.

The angle chosen for the glideslope was set at 9°, which is the same angle used in the initial descent of the experiments with the same UAV in [3]. Once the recovery maneuver completes, the plan loops back to the beginning for another repetition. Several versions of this plan were used, with different placement of the waypoints before the start of the recovery maneuver, to verify the convergence onto the desired glideslope. Different initial heights, and start positions both on the desired horizontal path and on either side of it, were tested. Different initial heading angles were also tested. The wind was low, mostly about 1 m/s.

TABLE I: Maneuver parameters

Parameter	**Value**
$k_{(T,V,p)}$	$10\,\frac{\%}{\mathrm{m/s}}$
$k_{(T,V,i)}$	$2\,\frac{\%/\mathrm{s}}{\mathrm{m/s}}$
T_{trim}	45%
$k_{(\theta,\alpha_n,p)}$	12
$k_{(\theta,\alpha_n,i)}$	$0.25\,\frac{\mathrm{rad/s}}{\mathrm{rad}}$
$k_{(\theta,q,p)}$	0.05s
θ_{trim}	1.5°
$k_{(\phi,\psi,p)}$	$1.5\,\frac{\tan(\mathrm{rad})}{\mathrm{rad}}$
$k_{(\psi,\Psi_n,p)}$	3.5
$k_{(\psi,\Psi_n,i)}$	0.3
Distance to enable integrators	300 m
Elevation offset 2402 MHz	6.0°
Elevation offset 2426 MHz	6.6°
Elevation offset 2480 MHz	6.1°

Distance measured by GNSS was used to determine

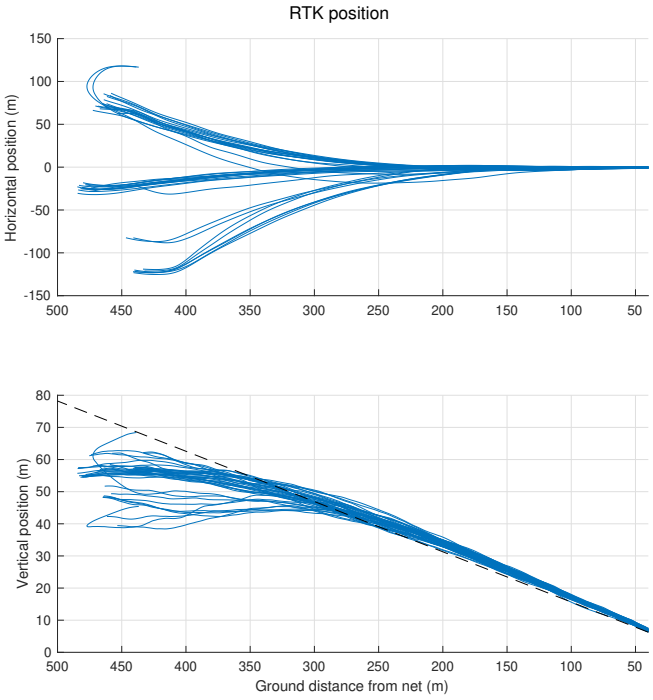

Fig. 10 UAV position plots from RTK GNSS for the 39 approaches. For some of the approaches the maneuver is initialized with a course angle error over 90°, such that the distance from the array is increasing.

when the recovery maneuver was deemed completed. A distance of 40 m was chosen to maintain a safe distance margin over the ground, corresponding to a net center position 6.3 m over the array. In total, 39 maneuvers were flown using Bluetooth navigation. The controller parameters used in the experiments are listed in Table I.

The RTK GNSS positions in the horizontal and vertical for all maneuvers are shown in Fig. 10. The position where the UAV would have impacted the net according to RTK GNSS is shown in Fig. 11. The spread in the impact position is not significantly worse than that achieved in stationary net experiments using RTK GNSS in [3]. A reasonably sized net, e.g. 5 × 5m, would have been hit for every attempt, with an RTK-indicated standard deviation of 0.41 m horizontally and 0.32 m vertically. The mean RTK GNSS impact position 0.45 m left of the desired point is likely the result of residual array azimuth calibration error, corresponding to a 0.67° error in the assumed azimuth angle. It does appear that the glideslope followed is slightly above the desired 9°, likely because of residual elevation calibration errors, resulting in impacts above the desired position. The position along the path calculated from Bluetooth direction and RTK GNSS distance is shown in Fig. 12. The noise in the direction estimate translates to a larger position noise for increasing range. The "sawtooth"-like pattern in the horizontal position is due to direction disagreement between the three Bluetooth channels used.

The elevation angles from RTK GNSS and Bluetooth direction finding are plotted against each other in

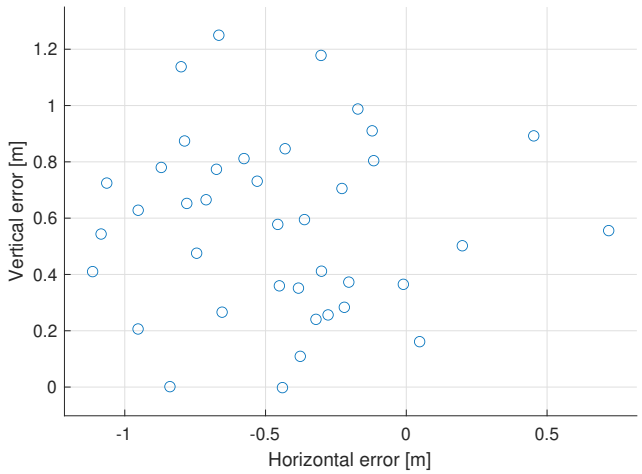

Fig. 11 Impact positions as seen from the glideslope towards the array, calculated from RTK GNSS position with the assumption of 128° azimuth and 10° elevation angle for the array orientation.

Fig. 13, showing the multipath effect on elevation angle estimation for the array setup used. Note the increased spread of the elevation measurements at elevation angles below the 9° glideslope. When the maneuver is initialized, the UAV is below the glideslope, as seen in Fig. 10. From the time when the maneuver is initialized until the UAV has reached the desired path the azimuth angle changes, which also changes the point on the ground where the signal reflects. Since the grass surface is not perfectly flat, the multipath effect on elevation can change in this period, resulting in the measurement spread observed.

VII. Conclusion

This paper has demonstrated the use of Bluetooth direction finding as a navigation system for automatic fixed-wing UAV recovery, suitable for arrest systems such as a suspended net. The multipath issue was taken into account, and the system has been shown capable of reliably hitting a stationary net without fusion with other sensors for navigation.

Acknowledgements

The authors are grateful for the support from Nordic Semiconductor, in particular Bjørn Spockeli, Paal Kastnes and Carsten Wulff. The authors also thank Terje Haugen for constructing the array leveling platform and UAV pilot Pål Kvaløy.

References

[1] R. Skulstad, C. Syversen, M. Merz, N. Sokolova, T. Fossen, and T. Johansen, "Autonomous net recovery of fixed-wing UAV with single-frequency carrier-phase differential GNSS," *Aerospace and Electronic Systems Magazine, IEEE*, vol. 30, no. 5, pp. 18–27, May 2015.

[2] H. J. Kim, M. Kim, H. Lim, C. Park, S. Yoon, D. Lee, H. Choi, G. Oh, J. Park, and Y. Kim, "Fully autonomous vision-based net-recovery landing system for a fixed-wing UAV," *IEEE/ASME Transactions on Mechatronics*, vol. 18, no. 4, pp. 1320–1333, Aug 2013.

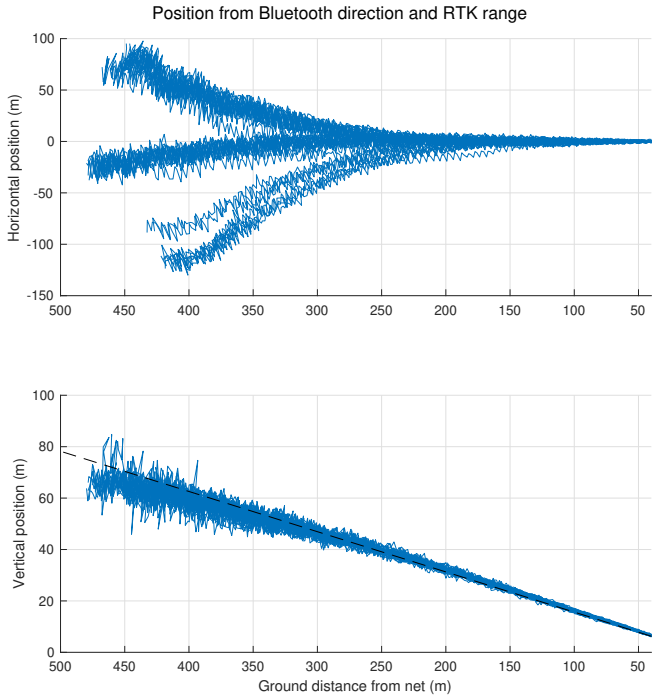

Fig. 12 UAV position plots from Bluetooth direction and RTK GNSS distance for the 39 approaches.

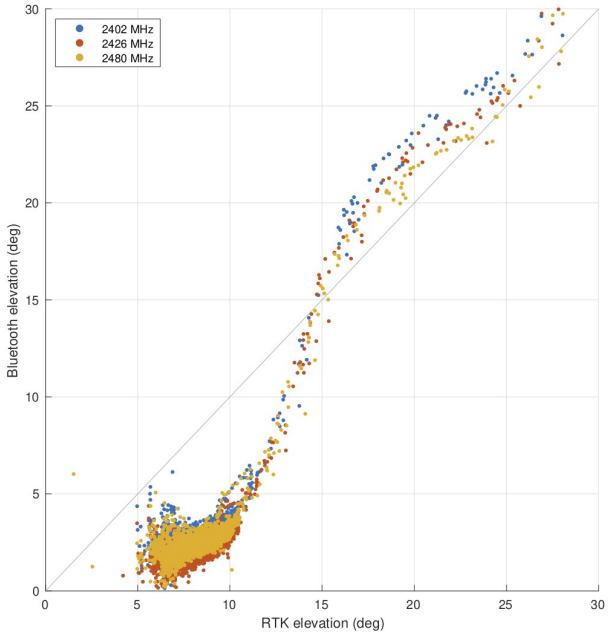

Fig. 13 Bluetooth elevation angle estimate vs. against elevation angle calculated from RTK GNSS.

[3] K. Gryte, M. L. Sollie, and T. A. Johansen, "Control System Architecture for Automatic Recovery of Fixed-Wing Unmanned Aerial Vehicles in a Moving Arrest System," *J. Intelligent and Robotic Systems*, vol. 103, no. 4, 2021.

[4] S. Khantsis and A. Bourmistrova, "Uav controller design using evolutionary algorithms," in *AI 2005: Advances in Artificial Intelligence*, S. Zhang and R. Jarvis, Eds. Berlin, Heidelberg: Springer Berlin Heidelberg, 2005, pp. 1025–1030.

[5] M. F. Bornebusch and T. A. Johansen, "Autonomous recovery of a Fixed-wing UAV Using a Line Suspended Between Two Multirotor UAVs," *IEEE Transactions on Aerospace and Electronic Systems*, vol. 9251, no. c, pp. 1–1, 2020.

[6] K. Klausen, T. I. Fossen, and T. A. Johansen, "Autonomous recovery of a fixed-wing UAV using a net suspended by two multirotor UAVs," *Journal of Field Robotics*, vol. 35, no. 5, pp. 717–731, 2018.

[7] W. Kong, D. Zhou, D. Zhang, and J. Zhang, "Vision-based autonomous landing system for unmanned aerial vehicle: A survey," in *Int. Conf. Multisensor Fusion and Information Integration for Intelligent Systems (MFI)*, 2014.

[8] Y. Lu, Z. Xue, G.-S. Xia, and L. Zhang, "A survey on vision-based UAV navigation," *Geo-spatial Information Science*, vol. 21, no. 1, pp. 21–32, 2018.

[9] S. Huh and D. H. Shim, "A vision-based automatic landing method for fixed-wing uavs," *Journal of Intelligent and Robotic Systems*, vol. 57, no. 1, p. 217, 2009.

[10] S. Thurrowgood, R. J. D. Moore, D. Soccol, M. Knight, and M. V. Srinivasan, "A biologically inspired, vision-based guidance system for automatic landing of a fixed-wing aircraft," *Journal of Field Robotics*, vol. 31, no. 4, pp. 699–727, 2014.

[11] K. Cisek, K. Gryte, T. H. Bryne, and T. A. Johansen, "Aided inertial navigation of small unmanned aerial vehicles using an ultra-wideband real time localization system," in *Proc. IEEE Aerospace Conference*, 2018.

[12] M. W. Mueller, M. Hamer, and R. D'Andrea, "Fusing ultra-wideband range measurements with accelerometers and rate gyroscopes for quadrocopter state estimation," in *IEEE International Conference on Robotics and Automation*. Seattle, Washington: IEEE, 2015, pp. 1730–1736.

[13] L. Botler, M. Spork, K. Diwold, and K. Romer, "Direction Finding with UWB and BLE: A Comparative Study," *Proc. IEEE 17th International Conference on Mobile Ad Hoc and Smart Systems (MASS)*, pp. 44–52, 2020.

[14] P. Bia, A. Calcaterra, D. Gaetano, C. Canestri, R. Ardoino, L. Scorrano, and A. Manna, "Compact Interferometric Antenna Array for UWB Direction Finding," in *34th General Assembly and Scientific Symposium of the International Union of Radio Science*, Rome, Italy, 2021.

[15] K. Gryte, T. H. Bryne, and T. A. Johansen, "Unmanned aircraft flight control aided by phased-array radio navigation," *Journal of Field Robotics*, vol. 38, no. 4, pp. 532–551, 2021.

[16] Z. HajiAkhondi-Meybodi, M. Salimibeni, A. Mohammadi, and K. N. Plataniotis, "Bluetooth low energy and cnn-based angle of arrival localization in presence of rayleigh fading," in *IEEE Int. Conf. Acoustics, Speech and Signal Processing (ICASSP)*, 2021, pp. 7913–7917.

[17] Z. Hajiakhondi-Meybodi, M. Salimibeni, K. N. Plataniotis, and A. Mohammadi, "Bluetooth low energy-based angle of arrival estimation via switch antenna array for indoor localization," in *FUSION*, 2020.

[18] M. L. Sollie, K. Gryte, T. H. Bryne, and T. A. Johansen, "Outdoor Navigation Using Bluetooth Angle-of-Arrival Measurements," *IEEE Access*, vol. 10, pp. 88 012–88 033, 2022.

[19] M. L. Sollie, "Navigation and automatic recovery of fixed-wing unmanned aerial vehicle," Ph.D. dissertation, Norwegian University of Science and Technology, Trondheim, Norway, 2022.

[20] M. L. Sollie, T. H. Bryne, K. Gryte, and T. A. Johansen, "Reducing ground reflection multipath errors for bluetooth angle-of-arrival estimation by combining independent antenna arrays," *IEEE Antennas and Wireless Propagation Letters*, vol. 22, pp. 1391–1395, 2023.

[21] S. M. Albrektsen and T. A. Johansen, "User-Configurable Timing and Navigation for UAVs," *Sensors*, vol. 18, no. 8, 2018.

[22] Laboratório de Sistemas e Tecnologia Subaquática - Faculdade de Engenharia da Universidade do Porto, "DUNE Unified Navigation Environment." [Online]. Available: https://www.lsts.pt/toolchain/dune

[23] Truerc.ca, "X-AIR 2.4." [Online]. Available: https://www.truerc.ca/shop/2-4ghz-2/receiver-long-range-2-4ghz-2/x-air-2-4